Preprint, Proceedings of the Combustion Institute, in press, 37, 2018.
https://doi.org/10.1016/j.proci.2018.07.046.

Ignition by moving hot spheres in H_2-O_2-N_2 environments

S. Jones[a,*], J. Melguizo-Gavilanes[a,b], J.E. Shepherd[a]

[a] *Graduate Aerospace Laboratories (GALCIT), California Institute of Technology, Pasadena, CA 91125, USA*
[b] *Institut Pprime, UPR 3346 CNRS, ISAE-ENSMA, BP 40109, 86961 Futuroscope-Chasseneuil Cedex, France*

Abstract

A combined experimental and numerical study was carried out to investigate thermal ignition by millimeter size (d = 6 mm) moving hot spheres in H_2-O_2-N_2 environments over a range of equivalence ratios. The mixtures investigated were diluted with N_2 to keep their laminar flame speed constant and comparable to the sphere fall velocity (2.4 m/s) at time of contact with the reactive mixture. The ignition thresholds (and confidence intervals) were found by applying a logistic regression to the data and were observed to increase from lean (Φ = 0.39; T_{sphere} = 963 K) to rich (Φ = 1.35; T_{sphere} = 1007 K) conditions. Experimental temperature fields of the gas surrounding the hot sphere during an ignition event were, for the first time, extracted using interferometry and compared against simulated fields. Numerical predictions of the ignition thresholds were within 2% of the experimental values and captured the experimentally observed increasing trend between lean and rich conditions. The effect of stoichiometry and dilution on the observed variation in ignition threshold was explained using 0-D constant pressure delay time computations.

Keywords:
hot particle ignition, hydrogen, interferometry, numerical simulation

*Corresponding author:
Email address: smjones@caltech.edu (S. Jones)

1. Introduction

There is a continuing interest in the aircraft, nuclear power, and chemical processing industries to investigate and understand the hazards associated with accidental ignition events [1]. Such events can lead to an explosion or other catastrophic failure of the craft or plant resulting in loss of life and infrastructure and a high environmental impact. Likely ignition sources in these scenarios are hot surfaces, both stationary and moving [2]. Experimental data on ignition thresholds by moving hot surfaces is scarce in the literature with the most recent data set published in the late 1930's and early 1940's [3, 4]. More recent data sets exist but for submillimeter stationary particles [5]. The ignition dynamics of undiluted stoichiometric hydrogen (H_2)-air, near and far from the ignition threshold, were numerically studied by Melguizo-Gavilanes et al. [6]. The investigation of the effects of differential diffusion [7] and particle velocity [8] on the numerical prediction of ignition thresholds were also the topic of recent research efforts. The present work will focus on investigating experimentally and numerically the ignition of nitrogen (N_2) diluted hydrogen-oxygen (H_2-O_2) mixtures by millimeter size (d = 6 mm) moving hot spheres. This study aims to provide: (i) new data on the ignition thresholds for hydrogen mixtures by moving hot particles; (ii) quantitative two-dimensional temperature fields of the gas surrounding the hot sphere during ignition; and (iii) numerical modelers with validated experimental ignition thresholds and quantitative two-dimensional temperature fields during an ignition event. Additionally, we comment on the implications of our results to the correlation proposed by Roth et al. [9].

2. Experimental methodology

The experiments were performed using the facility described in detail by Coronel [10]. A simplified schematic of the experimental setup is included in the Supplementary Materials. Briefly, a cylindrical stainless steel combustion vessel, with an internal volume of ~ 22 L is used. Windows are mounted on parallel flanges to allow for visualization of ignition. A heating chamber is located on top of the combustion vessel with an internal volume of ~ 0.1 L. The heating chamber has windows mounted on two parallel flanges, and on the other two sides has titanium supports, one of which is linearly actuated via a pneumatic piston. These supports are used to hold an alumina (Al_2O_3) sphere in place while it is being heated by a continuous wave 80 W carbon dioxide (CO_2) laser using a Proportional-Integral-Derivative (PID) controller. Al_2O_3 is chosen for its relative intertness. Extending from the bottom of the heating chamber into the interior of the combustion vessel is a hollow cylinder. A remotely actuated gate valve with an airtight seal is attached to the end of the hollow cylinder to fully isolate the cylinder and heating chamber from the combustion vessel. In previous experiments performed in our laboratory using n-hexane-air mixtures [10, 11], an optical shutter was sufficient to provide separation between inert and reactive mixture. In the current experiments, the airtight gate valve is critical to prevent hydrogen from diffusing into the heating chamber while the sphere is heated.
A blackbody-calibrated two-color pyrometer with an accuracy of ± 30 K makes non-contact measurements of the sphere surface temperature, T_{sphere}, and provides feedback to the PID controller. The controller adjusts the laser power output to achieve the desired T_{sphere}. Upon reaching the appropriate T_{sphere}, the actuated support retracts and the sphere falls into the hollow cylinder. A second pyrometer measures T_{sphere} at the end of the cylinder, just before it enters the reactive mixture. The gate valve is timed to open just before the sphere reaches it and lines up with the top of the field of view of the windows on the vessel. This allows the sphere to be visualized from the moment it enters the reactive environment. A shearing interferometer is used to visualize the falling sphere; the resulting interferograms are captured with a high-speed video camera at a rate of 13,000 frames per second. Image processing can be performed on the interferograms to obtain the temperature field around the sphere. Subsequently, the thermal boundary layer from an experiment can be directly compared to the thermal boundary layer predicted numerically. Additionally, T_{sphere} can be extrapolated from the thermal boundary layer data providing a way to cross-check the T_{sphere} readings from the pyrometer measurements. The capability of interferometry to provide quantitative temperature fields in the gas around the moving sphere is a significant advance. Previously, it had been used to qualitatively analyze ignition by stationary hot surfaces in undiluted hydrogen-air environments [12]. We now have demonstrated the extension of this method to quantitatively analyze ignition by moving particles in H_2-O_2-N_2 mixtures. Details of the interferometer configuration and image processing can be found in Coronel et al. [13].

3. Computational methodology

The motion, transport and chemical reaction in the gas surrounding the sphere were modeled using the variable-density reactive Navier-Stokes equations with temperature-dependent transport properties [14]. The computational methodology, spatial and temporal discretization details can be found in [7]. Thermal diffusion (Soret effect) and radiation were neglected in the current model. The chemistry was modeled using Mével et al. [15], Konnov [16], and GRI-Mech 3.0 [17] detailed mechanisms for hydrogen oxidation for the H_2-O_2-N_2 system using 9 species and 21, 27, and 27 reactions, respectively. Although these mechanisms were validated against extensive kinetics databases, they demonstrate significant differences in delay time predictions in the range of temperatures of interest [18]. Chemkin files for the Mével and Konnov mechanisms are provided in the Supplementary Materials. The Sutherland Law, Eucken relation and JANAF polynomials were used to account for the functional temperature dependence of mixture viscosity, thermal conductivity and specific heat, respectively. Mass diffusion fluxes were approximated using Fick's law and the mixture averaged binary diffusion coefficients [19].

The simulations were carried out with initial and boundary conditions that reproduce the experimental conditions described in section 2 as faithfully as possible. The numerical integration was divided in two parts: first, a free fall in N_2 for 0.25 s (fall time measured experimentally) during which a steady axisymmetric thermal boundary layer and wake develops; second, contact with reactive mixture (H_2-O_2-N_2 at Φ = 0.39, 1.0 and 1.35) for 20 ms (experimental observation duration) or until ignition is observed and initial stages of flame propagation take place. The time to ignition, t_{ign}, was determined by monitoring the maximum gas temperature in the computational domain during the numerical integration; when $T = T_{\text{sphere}} + 150$ K, $t = t_{\text{ign}}$. The results from [6] justify this choice as changing the threshold from +50 K to +650 K changed t_{ign} by < 0.1 ms. The numerical ignition thresholds were determined by systematically decreasing T_{sphere} from 1100 K in 20 K intervals until a self-sustained flame was no longer achieved. The computational domain consisted of a 5° wedge with a 2D-axisymmetric sphere located at $(0, 0)$ with diameter $d = 6$ mm. The axis of symmetry was located at $r = 0$ along the center of the sphere. The top, bottom and side boundaries were placed $15d$, $5d$ and $10d$ away from the center of the sphere, respectively. The domain was discretized using 300,000 cells with finer resolution near the sphere; a minimum cell size of 40 μm ensured that the thermal/hydrodynamic boundary layers were properly resolved. This resolution was selected as the result of a detailed grid resolution study, and validation for the inert model was shown in [13]. The initial conditions were $p_o = 100$ kPa, $T_o = 300$ K, $\mathbf{u}_o = (0, 0)$ m/s and a constant (uniform) T_{sphere} providing an isothermal boundary condition for the gas. The validity of this boundary condition was assessed using a Biot number analysis [20] and was found to satisfy the lumped capacitance assumption (Bi = 0.003). The temperature drop during the simulation test time was estimated to be less than 1% for the values of T_{sphere} considered. There is no net flux of species to the wall, and the effects of surface heterogeneous reactions were ignored. Buoyancy effects were neglected, as this represents a forced convection case ($\text{Gr}/\text{Re}^2 = 0.02 \ll 1$). The frame of reference was attached to the sphere, hence, a time dependent inflow boundary condition of $\mathbf{u}(t) = (0, gt)$ was prescribed at the bottom of the computational domain to properly simulate the fall of the heated sphere. At the top, a non-reflective/pressure transmissive boundary condition was used to simulate an outflow. A schematic showing the simulation setup was included in a previous study [6] and is given in the Supplementary Materials. The governing equations were solved using the Open source Field Operation And Manipulation (OpenFOAM) toolbox [21]. Our implementation of the code has been validated in various ignition studies comprising different geometries, modes of heat transfer (i.e. forced and natural convection), and ignition timescales [6, 7, 12, 22].

4. Results and Discussion

4.1. Ignition thresholds

Three mixtures were tested experimentally at equivalence ratios of Φ = 0.39, 1.0, and 1.35. The initial composition is specified as $2\Phi H_2 + O_2 + \beta N_2$. The values of Φ and β for lean, stoichiometric and rich conditions are Φ = 0.39, β = 2.97; Φ = 1, β = 9; and Φ = 1.35, β = 11.84, respectively. These mixtures were selected to keep the computed laminar burning speed s_L^0 constant. The value of s_L^0 = 0.35 m/s was chosen so that the flame speed, $u_f = s_L^0 \rho_u/\rho_b$ (where ρ_u and ρ_b are the unburnt and burnt gas densities, and the ratio of ρ_u/ρ_b = 4.9, 4.87 and 4.19 for Φ = 0.39, 1.0 and 1.35 respectively), was comparable but not equal to the sphere fall velocity of 2.4 m/s at the time of contact with reactive mixture. This enabled capturing the ignition process and early stages of flame propagation using interferometry for all conditions. The experimental ignition thresholds

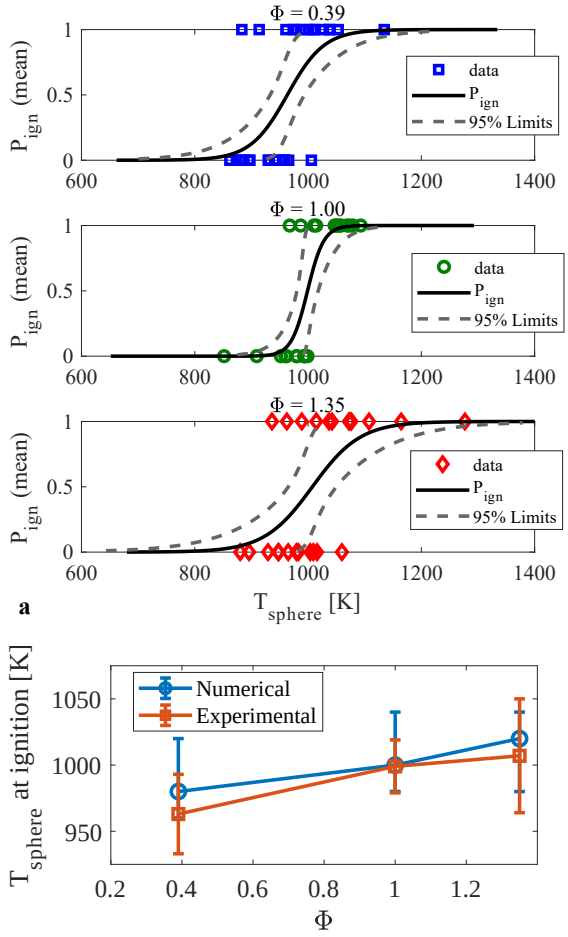

Figure 1: a.: probability of ignition (P_{ign}) derived from experimental data, markers represent data points. b.: experimental and numerical ignition threshold results - experimental bounds given by width of 95% confidence intervals; numerical upper and lower bounds given by Konnov and GRI-Mech 3.0 respectively.

reported correspond to T_{sphere} at which a 50% probability of ignition was observed. These probabilities were found by performing a logistic regression analysis on the experimental data, about 30 tests per mixture, using T_{sphere} as the independent variable and a binary outcome as the dependent variable with one (1) representing an ignition, and zero (0) a no-ignition event. A detailed description of the method used to compute probabilities can be found in Bane et al. [23]. Figure 1a shows probability of ignition curves for the three mixtures investigated experimentally. For lean conditions (Φ = 0.39) the ignition threshold was 963 K with a confidence interval (95%) of ± 30 K; for stoichiometric conditions (Φ = 1.0) we obtained 999 K with a confidence interval of ± 20 K; for rich conditions (Φ = 1.35), 1007 K with a confidence interval of ± 43 K.

The ignition threshold was found to increase as a function of Φ from lean to rich conditions. This increase is noticeable when comparing thresholds, but the confidence intervals for each experimental mixture overlap. Note that the pyrometer measurement has an uncertainty of ± 30 K, which has not been taken into account in the computation of confidence intervals. Figure 1b shows a comparison of the experimental and numerical results together with experimental and numerical upper and lower bounds on the ignition thresholds. The experimental bounds are due to the confidence intervals of the logistic regression, while the numerical bounds were obtained by finding the ignition thresholds using the three different chemical kinetics detailed mechanisms mentioned in section 3. Presenting the numerical results in this fashion has the advantage of showing the sensitivity of numerical predictions to the chemical mechanism used. Using the Mével mechanism results in thresholds of 980 K (+40/-20) for Φ = 0.39, 1000 K (+40/-20) for Φ = 1.0 and 1020 K (+20/-40) for Φ = 1.35. The values in parentheses correspond to the upper and lower bounds predicted by using Konnov and GRI-Mech 3.0, respectively. While Mével's mechanism predicts an increasing trend as a function of Φ in the range considered in this study, the ignition thresholds for Konnov and GRI-Mech 3.0 remain constant for $\Phi \geq 1.0$. Obtaining increasing ignition thresholds with increasing Φ is in agreement with our current experimental results, and the experimental and numerical observations of Roth et al. [5] using stationary submillimeter particles.

The differences between experimental and predicted ignition temperature thresholds using the Mével mechanism are 1.8%, 0.1% and 1.3% for Φ = 0.39, 1.0 and 1.35, respectively. The numerical simulation predicts the trend observed experimentally between lean and rich conditions. This gives confidence that the numerical model can be used as a predictive tool for determining ignition thresholds. The maximum difference in ignition threshold observed in the numerical predictions when using different kinetic mechanisms is 40 K. Coincidentally, neglecting differential diffusion effects in undiluted stoichiometric hydrogen-air also causes a change of 40 K in the ignition threshold [7]. This suggests that for H_2-O_2-N_2 mixtures, both differential diffusion and choice of kinetic mechanism should be accounted for to make accurate predictions of the ignition threshold.

4.2. *Temperature fields*

The physical and chemical processes important to the ignition dynamics occur within the thermal boundary

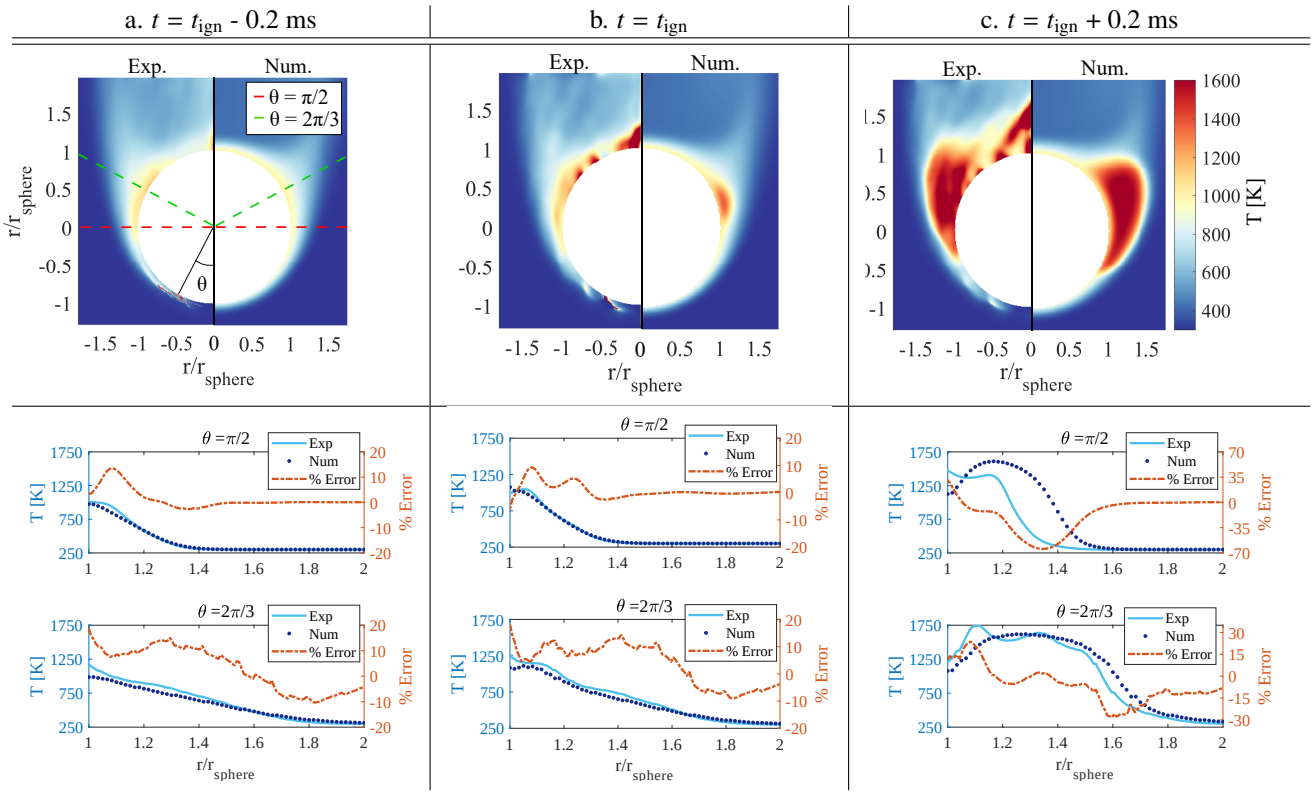

Figure 2: Ignition dynamics for a critical case with $\Phi = 1, \beta = 9$: a. shortly before ignition, $t = t_{ign}$ - 0.2 ms; b. at ignition, $t = t_{ign}$; and c. during early stages of flame propagation, $t = t_{ign}$ + 0.2 ms. Length scale, r_{sphere} = 3 mm. Top row: experimental (T_{sphere} = 989 ± 30 K) and numerically predicted (T_{sphere} = 1000 K) gas temperature fields. All temperature fields share a common colorbar, shown in Fig. 2c (top row). Bottom row: comparison of experimental and numerical thermal boundary layer and error profiles at $\theta = \pi/2$ (top) and $2\pi/3$ (bottom).

layer near the sphere surface [6]. Simulating these processes requires careful attention to grid resolution near the sphere boundary and modeling the chemical reaction and transport processes with high fidelity. Previous studies have included investigation of the chemical structure of the flame kernel[6, 7]. Verification of these types of complex simulations is challenging so we have carried out extensive validation of the solver against the experimental results of [5, 24, 25]. A temperature field validation of an ignition event is shown in Fig. 2 for Φ = 1.0 and $\beta = 9$. Later times were simulated, but we chose to focus on the ignition transient as stated in the objectives of this study. Figure 2a is constructed from averaging frames for $t_{ign} - 1.7$ ms $\leq t \leq t_{ign} - 0.2$ ms. Time averaging is appropriate because the thermal boundary layer is steady just before ignition occurs. The images in Fig. 2b and c (top row) are individual frames taken $\sim$ 0.2 ms apart to capture ignition and early stages of flame propagation. Note that Fig. 2b and c are noisy because the interferograms are taken during the transient ignition event and therefore time averaging cannot be performed over multiple images [13]. Nonetheless, the ignition event can still be clearly observed. Figure 2a shows the temperature field shortly before ignition. It is evident that interferometry is capable of capturing many of the key features in the thermal boundary layer, such as its growth from the front stagnation point to the separation region, as well as the shape of the wake. The thermal boundary layer varies in thickness from 0.5 to 2 mm, and with interferometry we are able to infer gas temperatures as close as 24 μm to the sphere. Figure 2b shows the ignition kernel forming near the separation region and Fig. 2c shows the flame propagating outwards into fresh reactants. The predicted flame temperature in the 2-D simulations of 1692 K is in agreement with the experimentally inferred average value of 1650 K. This is the first time that this imaging technique has been used to reconstruct an ignition event for moving particles. These are encouraging results that indicate the utility of interferometry for resolving transient combus-

tion events. Note that for the temperature fields shown, there are discrepancies near the front and back stagnation points. The challenges encountered resolving these regions are discussed in Coronel et al. [13]. Further refinement of the windowing technique [13] used in the post-processing or averaging over multiple experiments may help reduce the noise inherent from processing a single image, and enable more accurate reconstruction of flames and ignition events. Figure 2a-c (bottom row) shows a comparison of the radial distribution of temperature normal to the sphere surface and the deviation (% Error) between the experimental and numerical thermal profiles at $\theta = \pi/2$ and $\theta = 2\pi/3$; the front stagnation point is $\theta = 0$. Properly resolving the thermal boundary layer in this range of θ is important because it is precisely in this region where ignition is experimentally observed and numerically predicted to occur when T_{sphere} is close to the ignition threshold (critical case). The temperature distributions are extracted at locations along the dashed lines shown in Fig. 2a. A sphere surface temperature of 1007 K is extrapolated from the experimental profile. This is in agreement with the pyrometer measurement of 989 K, well within the calibration uncertainty. Close agreement between the pyrometer readings and interferometer surface temperature measurements give additional confidence in the accuracy of the measured surface temperatures. The average deviations computed at the two locations sampled (see orange line in Fig. 2 - bottom row) were less than 10% for $t = t_{\text{ign}}$ - 0.2 ms and $t = t_{\text{ign}}$, and as expected are larger for $t = t_{\text{ign}}$ + 0.2 ms. These results, combined with the spatial and temporal resolution achieved (24 μm and 77 μs respectively) indicate that interferometry is a sufficiently accurate technique for studying ignition transients experimentally. A more detailed discussion of the advantages of the technique and a thorough error analysis of the experimentally obtained temperature fields was performed in [13], accounting for both algorithm error and noise in the interferograms. Additional ignition sequences for the other concentrations considered are shown in the Supplementary Materials.

4.3. Effect of β and Φ on ignition thresholds

To isolate chemical effects and further understand the influence of initial composition on the trends observed in ignition threshold, 0-D constant pressure delay time calculations were performed using Cantera [26]. We expect that all other factors being the same, a mixture with a longer ignition delay time at a given temperature will have a higher ignition temperature threshold than one with a shorter ignition delay time under the same conditions. The delay time, τ, was computed as a function of β and Φ, the initial conditions used were p_o = 100 kPa, T_o = 1000 K, and the chemistry was modeled using Mével's mechanism. Note that the temperature value chosen corresponds to the sphere surface temperature at the nominal ignition threshold (see Fig. 1). The ignition delay time was extracted by selecting the time at which the concentration of OH reached a maximum. The results of these computations are shown in Fig. 3. Increasing β at a fixed Φ leads to longer ignition delay times. This is an expected effect as increasing the amount of diluent effectively decreases the rate at which potentially reactive collisions occur; N_2 dominates most collisions. Conversely, increasing Φ at a fixed β decreases τ by about 10%. The coupled effect that increasing both β and Φ has on the experimental mixtures is apparent. Increasing β from 2.97 to 9.0 at $\Phi = 0.39$ more than doubles the delay time from 0.20 ms to 0.46 ms. At $\beta = 9.0$, increasing Φ from 0.39 to 1.0 decreases the delay time from 0.46 ms to 0.41 ms. This trend of an overall increase in delay time repeats as β and Φ increase to 11.84 and 1.35, respectively. Consequently, while both dilution and equivalence ratio have an effect on ignition delay time, the effect of dilution dominates for the mixtures considered in this study. This explains the increase in ignition threshold observed experimentally and numerically. The simplified description of a chain branching explosion as discussed by Sánchez and Williams [27] offers another explanation. Their model for ignition delay time is inversely proportional to the concentration of O_2. This model also predicts an increasing trend of ignition delay time as a function of equivalence ratio because the increasing dilution level and equivalence ratio lead to a decrease in O_2 concentration.

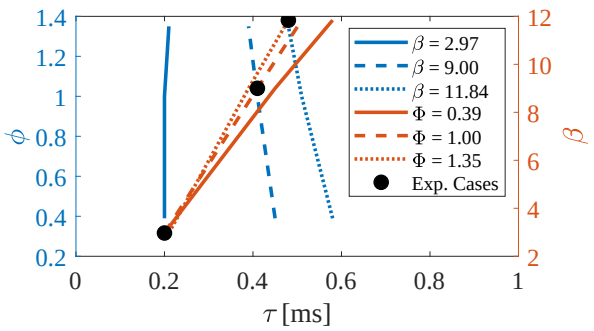

Figure 3: Effect of changing β and Φ on ignition delay time, τ, from 0-D constant pressure computations. Blue lines (solid, dashed and dotted) represent the effect of varying Φ at a fixed β; orange lines (solid, dashed and dotted) represent the effect of varying β at a fixed Φ; black markers represent the composition of experimental cases.

4.4. Comparison of ignition thresholds

Performing these experiments with a constant s_L^0 allowed us to examine the correlation proposed by Roth et al. [9] who showed that s_L^0 at stoichiometric conditions for various fuels could be correlated with the ignition threshold. In Fig. 4 we plot our results together with Roth et al. [9], Haeber et al. [28] and Boeck et al. [29] results for H_2-O_2-N_2 mixtures. The results of Roth et al. were obtained using submillimeter stationary laser heated particles of d = 0.8 mm for Φ = 1.0, the results of Haeber et al. were obtained for 2D simulations of stationary linearly heated particles of d = 0.8 mm for $0.1 \leq \Phi \leq 3.5$, and the results of Boeck et al. were obtained using stationary vertical and horizontal cylinders of d = 10 mm for $0.1 \leq \Phi \leq 6.8$. The error bars represent the confidence intervals of Roth et al., the variation in threshold as a function of Φ reported by Haeber et al. and the pyrometer measurement uncertainty of Boeck et al. A few features stand out from this plot: (i) the effect of size of the hot surface at ignition is evident when comparing Boeck et al. and Roth et al. results. An increase of ~ 100 K in ignition threshold was found for a decrease in hot surface size from 10 to 0.8 mm for stoichiometric H_2-O_2-N_2 mixtures. Tests with very different surface sizes but the same s_L^0 yield two different ignition thresholds with error bars that do not overlap; (ii) in the present study, a fixed s_L^0 but different values of Φ resulted in thresholds that are weakly dependent on Φ, with a ΔT = 44 K from lean to rich conditions, but are much lower than the values that would be predicted if the correlation of Roth et al. were to be used; (iii) the values plotted for Boeck et al. with dashed error bars include the variation in threshold as a function of orientation (i.e. horizontal: 960 - 1100 K; vertical: 980 - 1115 K) and Φ. The thresholds for H_2-O_2-N_2 mixtures seem to be independent of orientation, and only weakly dependent on Φ away from the flammability limits. This is consistent with the findings of Haeber et al. Note that within the flammability limits in H_2-air, s_L^0 varies by ~28 times, yet the surface temperature at ignition only varies by 130 K [12]. This range is comparable to the size of the confidence bounds reported by Roth et al. at Φ = 1.0; (iv) the effect of motion, moving vs. stationary hot surfaces, is not clear from the plot as one would expect higher ignition thresholds for moving particles, and we observe the opposite when comparing our results with those reported by Roth et al. Note however that previous work has shown [5] that as the particle diameter drops below 1 mm, the surface temperature needed to achieve ignition increases sharply, hence the effect of size dominates over that of forced convection in the regime we have examined.

These experimental observations and theoretical considerations indicate that it will be challenging to correlate ignition thresholds with a single parameter like s_L^0. Thermal ignition is a complex phenomenon, and the interaction of the flow with the hot surface plays an important role in creating regions prone to ignition [6, 12]. Additionally, diffusion of light species away from the ignition center [7], the decomposition of large fuels into lighter more reactive fuels [11], and as discussed above, the size and motion of the hot surface with respect to the surrounding gas [12, 22] also play an important role. These studies as well as the present work are part of an ongoing effort to formulate a general thermal ignition framework. However, a discussion of this formulation is outside the scope of the present paper.

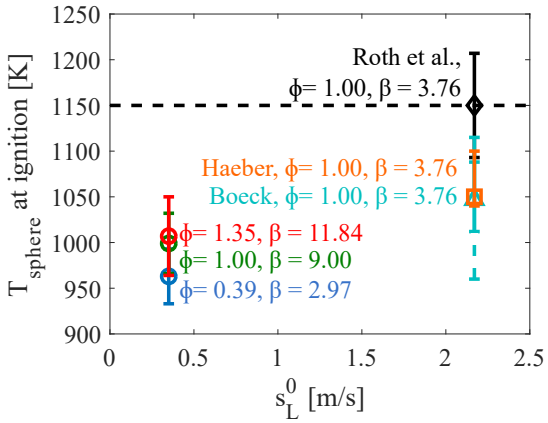

Figure 4: Ignition thresholds from this work plotted with that of Roth et al. [9], Haeber et al. [28] and Boeck et al. [29] for hydrogen mixtures as a function of laminar flame speed, s_L^0.

5. Conclusion

Thermal ignition by moving spheres (d = 6 mm) in H_2-O_2-N_2 environments was investigated in a combined experimental and numerical study. The experimental ignition thresholds were found to slightly increase as a function of Φ from 963 ± 30 K at Φ = 0.39 to 1007 ± 43 K at Φ = 1.35. The numerical simulations predicted thresholds that were within 2% of the experimentally determined values. The effect of varying the kinetic mechanism was assessed and included in the numerical results as uncertainty ranges. This work also presented a significant advance in the use of interferometry: quantitative temperature fields of ignition by a moving particle were obtained. The experimental temperature fields before, during and after ignition were compared

against numerical predictions and very encouraging results were obtained. Future work will focus on noise reduction by refining the image processing algorithm and by averaging across multiple experiments. Finally, the correlation by Roth et al. [9] was considered with the ignition thresholds found in this work and from Haeber et al. [28] and Boeck et al. [29]. Mixtures with the same s_L^0 tested with various sizes and configurations of hot surfaces had different ignition thresholds. Furthermore, within the range of Φ studied by Boeck alone, s_L^0 varied significantly (28 times), while the surface temperature at ignition only changed by 130 K, leading to a very weak dependence of the ignition threshold on s_L^0. This evidence suggests that drawing a correlation between T_{sphere} at ignition and s_L^0 does not account for a variety of phenomena that can have an effect on ignition and should be used cautiously.

Acknowledgements

Special thanks to Stephanie Coronel for her development of the interferometry processing software and the experimental apparatus, and to Lorenz Boeck for his design of the gate valve. Research carried out in the Explosion Dynamics Laboratory and supported by The Boeing Company (CT-BA-GTA-1). This work used the Extreme Science and Engineering Discovery Environment (XSEDE), which is supported by National Science Foundation grant number ACI-1548562.

References

[1] B. Stack, A. Sepeda, M. Moosemiller, Process Safety Progress 33 (2014) 19–25.
[2] V. Babrauskas, Ignition handbook, Fire Science Publishers, Issaquah, WA, 2003.
[3] R. S. Silver, The London, Edinburgh, and Dublin Philosophical Magazine and Journal of Science 23 (1937) 633–657.
[4] S. Paterson, The London, Edinburgh, and Dublin Philosophical Magazine and Journal of Science 30 (1940) 437–457.
[5] D. Roth, P. Sharma, T. Haeber, R. Schiessl, H. Bockhorn, U. Maas, Combustion Science and Technology 186 (2014) 1606–1617.
[6] J. Melguizo-Gavilanes, S. Coronel, R. Mével, J. Shepherd, International Journal of Hydrogen Energy 42 (2017) 7380–7392.
[7] J. Melguizo-Gavilanes, R. Mével, S. Coronel, J. Shepherd, Proceedings of the Combustion Institute 36 (2017) 1155–1163.
[8] T. Zirwes, F. Zhang, T. Häber, D. Roth, H. Bockhorn, Combustion Science and Technology (in press, 2018) (2018) 1–18.
[9] D. Roth, T. Häber, H. Bockhorn, Proceedings of the Combustion Institute 36 (2017) 1475–1484.
[10] S. A. Coronel, Thermal Ignition Using Moving Hot Particles, Ph.D. thesis, California Institute of Technology, 2016.
[11] S. A. Coronel, J. Melguizo-Gavilanes, R. Mével, J. E. Shepherd, Combustion and Flame 192 (2018) 495–506.
[12] J. Melguizo-Gavilanes, L. Boeck, R. Mével, J. Shepherd, International Journal of Hydrogen Energy 42 (2017) 7393–7403.
[13] S. A. Coronel, J. Melguizo-Gavilanes, S. Jones, J. E. Shepherd, Experimental Thermal and Fluid Science 90 (2018) 76–83.
[14] T. Poinsot, D. Veynante, Theoretical and Numerical Combustion, Edwards, 2005.
[15] R. Mével, S. Javoy, G. Dupré, Proceedings of the Combustion Institute 33 (2011) 485–492.
[16] A. Konnov, Detailed reaction mechanism for small hydrocarbons combustion. release 0.5., 2000.
[17] G. Smith, D. Golden, M. Frenklach, N. Moriarty, B. Eiteneer, M. Goldenberg, C. Bowman, R. Hanson, S. Song, W. Gardiner, V. Lissianski, Z. Qin, Gri-mech release 3.0, 1999.
[18] R. Mével, J. Melguizo-Gavilanes, L. Boeck, A. Nové-Josserand, Y. Kishita, S. Coronel, J. Shepherd, Proceedings of the Eleventh International Symposium on Hazard, Prevention, and Mitigation of Industrial Explosions (2016).
[19] R. J. Kee, M. E. Coltrin, P. Glarborg, Chemically reacting flow: theory and practice, John Wiley & Sons, 2005.
[20] F. Incropera, D. DeWitt, Fundamentals of Heat and Mass Transfer, Wiley, New York, 1996.
[21] H. G. Weller, G. Tabor, H. Jasak, C. Fureby, Computers in Physics 12 (1998) 620–631.
[22] J. Melguizo-Gavilanes, P. Boettcher, A. Gagliardi, V. Thomas, R. Mével, US National Combustion Meeting (2015).
[23] S. Bane, J. Shepherd, E. Kwon, A. Day, International Journal of Hydrogen Energy 36 (2011) 2344–2350.
[24] M. Beyer, D. Markus, Science and Technology of Energetic Materials: Journal of the Japan Explosive Society 73 (2012) 1–7.
[25] E. Brandes, W. Möller, B. P.-T. Bundesanstalt, Characteristic Data: Volume 1: Flammable Liquids and Gases, Fachverlag NW in Carl Ed. Schünemann KG., 2008.
[26] D. G. Goodwin, H. K. Moffat, R. L. Speth, Cantera: an object-oriented software toolkit for chemical kinetics, thermodynamics, and transport processes, 2017.
[27] A. Sánchez, F. Williams, Progress in Energy and Combustion Science 41 (2014) 1–55.
[28] T. Haeber, T. Zirwes, D. Roth, F. Zhang, H. Bockhor, U. Maas, Zeitschrift fur Physikalische Chemie 231 (2017) 1625–1654.
[29] L. R. Boeck, M. Meijers, A. Kink, R. Mével, J. E. Shepherd, Combustion and Flame 185 (2017) 265–277.